Modeling Hot-Electron Gate Current in Si MOSFET's Using a Coupled Drift-Diffusion and Monte Carlo Method

Chimoon Huang, Tahui Wang, C. N. Chen, M. C. Chang, and J. Fu

Abstract—**A coupled two-dimensional drift-diffusion and Monte Carlo analysis is developed to study the hot-electron-caused gate leakage current in Si n-MOSFET's. The electron energy distribution in a device is evaluated directly from a Monte Carlo model at low and intermediate electron energies. In the portion of high electron energy where the distribution function cannot be resolved by the Monte Carlo method due to limited computational resources, an extrapolation technique is adopted with an assumption of a Boltzmann tail distribution. This assumption is based on the simulation result that although the distribution function at a high electric field shows a markedly non-Maxwellian feature globally, it has approximately an exponential decay in an energy region much above average electron energy. A particular averaging method is employed to extract the effective electron temperature in the extrapolation. Our result shows that the electron temperature obtained in this approach is about three times lower than that derived from average electron energy by means of $\langle E \rangle = 3/2\ kT_e$ in the high-field domain of a device. Channel hot electron injection into a gate via quantum tunneling and thermionic emission is simulated. Electron scattering in gate oxide is also taken into account. The calculated values of gate current are in good agreement with experimental results. In the simulation, the most serious hot electron injection occurs about 200–300 Å behind the peak of average electron energy due to a delayed heating effect.**

I. Introduction

As THE Si MOSFET technology is moving rapidly into deep-submicrometer domain, hot-electron-induced phenomena have spurred great research interest because of their important role in device reliability and characterization [1]–[4]. Channel hot electron injection (CHEI) into a gate has been widely recognized as a major cause for device performance degradation due to electron trapping in gate oxide and/or interface states generation.

Manuscript received March 23, 1992; revised May 18, 1992. This work was supported by the National Science Council, ROC, under Contract NSC81-0404-E-009-106 and by the Electronics Research Service Organization (ERSO), ITRI, ROC. The review of this paper was arranged by Associate Editor A. H. Marshak.

C. Huang and T. Wang are with the Institute of Electronics, National Chiao-Tung University, Hsin-Chu, Taiwan, ROC.

C. N. Chen, M. C. Chang, and J. Fu are with the Electronic Research and Service Organization, Industrial Technology Research Institute, Hsin-Chu, Taiwan, ROC.

IEEE Log Number 9202309.

Many theoretical and experimental techniques have been developed to explore the physics of CHEI in terms of a gate leakage current [5]–[8]. Conventional hot electron theories based on stationary transport usually assume a local and instantaneous equilibrium between electric field and electron energy [9]. Thus electric field rather than electron energy is chosen as a primary variable to evaluate hot-electron effects. Since the CHEI mechanism is intrinsically related to an energy distribution, such an assumption may lead to quite different interpretations or conclusions about hot electron behavior in submicrometer devices. Therefore, more advanced transport models involving electron energy become mandatory for a rigorous analysis of the hot-electron effects.

Various modifications on hot electron simulation methods have been proposed to tackle the deficiencies of the conventional models. Hu *et al.* were first to use the "lucky electron" concept to empirically explore a gate current [6]. In their model, various parameters are determined in order to take into account the rapid spatial variation of electric field. Subsequently, Kuhnet *et al.* improved the lucky electron model to incorporate the nonlocal effect [10]. Frey [11] and Hoffman [12] utilized energy transport to calculate the substrate and gate currents in the devices. Recently, Riccò *et al.* have derived a numerical gate current model to further take into account the non-Maxwellian form of the distribution function [13]. However, a parabolic band structure [13] and a constant mean free path are two disputed assumptions in the models [8], [12]. These two assumptions are obviously inappropriate in the case of the CHEI since extremely high energy electrons (a few electronvolts) are usually involved. In addition, a Maxwellian distribution with a single electron temperature calculated from average electron energy is commonly observed in the previous models.

More recently, an ensemble Monte Carlo (EMC) method has been developed to simulate hot-electron transport in Si MOSFET's [14]–[16]. According to the EMC results, the electrons in the high-field domain of a device have a strong non-Maxwellian distribution. A single electron temperature is not adequate to describe the whole electron distribution function. This assertion virtually

contradicts the previous modeling approaches which were on a basis of a single electron temperature [11], [12], [17].

Although the EMC method has been successfully applied to modeling a substrate current in n-MOSFET's [14], it is CPU-time prohibitive to use the EMC method to calculate directly the CHEI effect in the entire energy region of interest. The difficulty arises because the CHEI is caused by electrons with energy about the Si/SiO_2 interface barrier height $\phi_0 = 3.2$ eV, while the energy threshold for hot-electron impact ionization in modeling a substrate current is only 16 eV. In this paper, we propose a simple and efficient method to approximate the high-energy tail distribution in the devices.

Our method is based on the findings from the EMC simulation that although the distribution function shows a markedly non-Maxwellian picture globally, the high-energy portion of the distribution function (i.e., an energy region much above average electron energy) exhibits a strong resemblance to a Boltzmann tail. An extrapolation of the EMC-calculated distribution with an assumption of a Boltzmann tail distribution can be used to overcome the Monte Carlo limit imposed by available computational resources. However, it should be emphasized that the high-energy tail in the extrapolation can no longer be characterized by the electron temperature derived from the average electron energy $\langle E \rangle$. Instead, a particular averaging technique to extract the effective temperature for the tail distribution will be discussed in the following section.

In our analysis, the CHEI via quantum-mechanical tunneling and thermionic emission is modeled. The tunneling probability is calculated by the WKB approximation with the band diagram evaluated from a general two-dimensional (2D) device simulator. Electron scattering in the gate oxide is also considered.

II. Simulation Model

The basic scheme of this work is to use a 2D device simulator, Silvaco PISCES IIB [18], to calculate the electric field distribution in a Si n-MOSFET. A Monte Carlo window is positioned as illustrated in Fig. 1 such that all possible CHEI trajectories are included in the window. x is in the channel direction and y is in the direction perpendicular to the channel. Sample electrons are launched from the left boundary of the window according to the electron concentration distribution from PISCES IIB. The launched electrons have a room temperature and a Maxwellian distribution in energy. The lower and upper surfaces of the Monte Carlo window are treated as a reflective boundary. In other words, electrons are bounced back if they encounter the boundaries.

A. Monte Carlo Model

A realistic pseudopotential band structure as described by Tang and Hess [16] is incorporated in the EMC model. The scattering mechanisms are acoustic phonon scattering, intervalley optical phonon scattering, and impact ionization. The Keldysh model is used to calculate the electron impact ionization rate [19]. Details of the Monte Carlo simulation including a Si pseudopotential band structure can be found elsewhere [14], [16]. As far as the CHEI is concerned, we calculate the electron distribution function along the Si/SiO_2 interface $f(x, E)$. In the simulation, as a sample electron hits the Si/SiO_2 interface, it is recorded in a counter $N_c(x)$ according to its position. The total number of electrons reaching the drain is also accumulated in an estimator N_{tot}. The average probability that a sample electron impinges on the Si/SiO_2 interface is $P_c(x) = N_c(x)/N_{tot}$. Once the electron distribution function $f(x, E)$ and the collision probability $P_c(x)$ are obtained, the electron injection probability into a gate $P_{inj}(x)$ can be expressed as

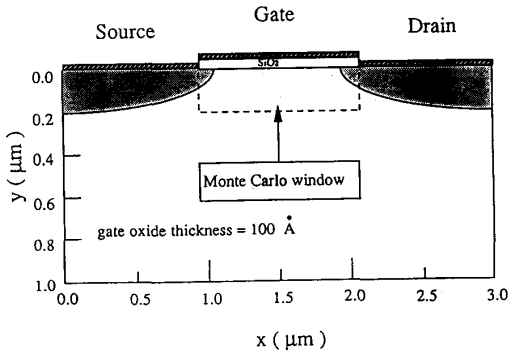

Fig. 1. Schematic representation of the simulated MOSFET structure and the Monte Carlo window.

$$P_{inj}(x) = \int_0^\infty P_c(x) f(x, E) D(E) P_t(x, E)\, dE \qquad (1)$$

where $D(E)$, plotted in Fig. 2, is the electron density of states associated with the Si pseudopotential band structure. $f(x, E)$ is normalized such that

$$\int f(x, E) D(E)\, dE = 1.$$

$P_t(x, E)$ denotes the oxide transmission probability. The current loss due to phonon scattering in the gate oxide layer is also included in $P_t(x, E)$. Integrating (1) along the channel, the resulting gate leakage current is obtained

$$I_g = I_{ds} \int_{channel} P_{inj}(x)\, dx. \qquad (2)$$

B. Electron Distribution Function

The probability that a channel electron reaches the gate electrode can be estimated as the ratio of the gate current to the drain current. In realistic devices, the typical values of this ratio are on the order of magnitude of 1.0×10^{-9}. A statistically meaningful result cannot be achieved in an EMC simulation unless a very large number of sample electrons is simulated. For example, 10^{10} sample electrons must be injected from the source to have about 10 electrons reaching the gate. Fig. 3 shows the Monte Carlo calculated distribution function $f(x, E)$ at $x = 1.7$ μm and

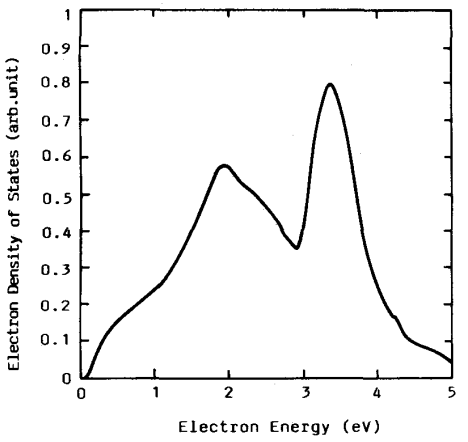

Fig. 2. The electron density of states associated with the pseudopotential band structure in Si.

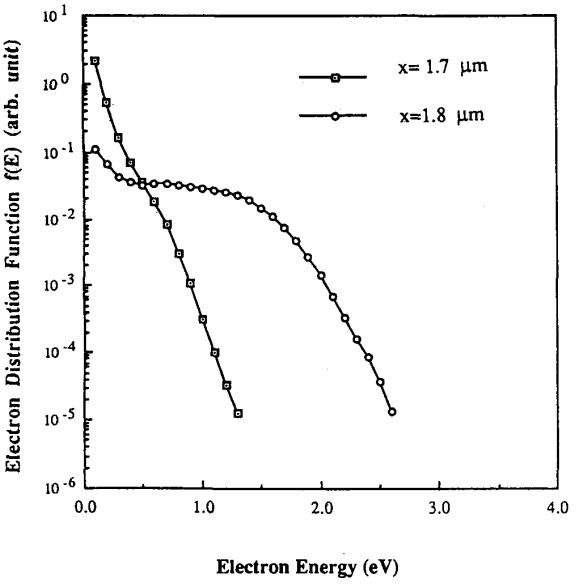

Fig. 3. The Monte Carlo calculated electron distribution functions at the Si/SiO_2 interface.

$x = 1.8$ μm in the n-MOSFET structure of Fig. 1. The structure has an effective channel length of 0.8 μm, a gate oxide thickness of 100 Å, a junction depth of 0.2 μm, a gate width of 20 μm, and a channel doping of 10^{16} cm^{-3}. The two-dimensional electric field profile in the device at $V_g = 5$ V and $V_d = 6$ V is shown in Fig. 4. It is found in Fig. 3 that the electron distribution at $x = 1.7$ μm (before strong field heating) follows approximately a Maxwellian distribution (i.e., a straight line in a logarithmic scale). In the high-field region, the distribution function ($x = 1.8$ μm curve) significantly deviates from the Maxwellian distribution around the average energy and has an exponential decay again with a slope of $-1/kT_e'$ in a region much

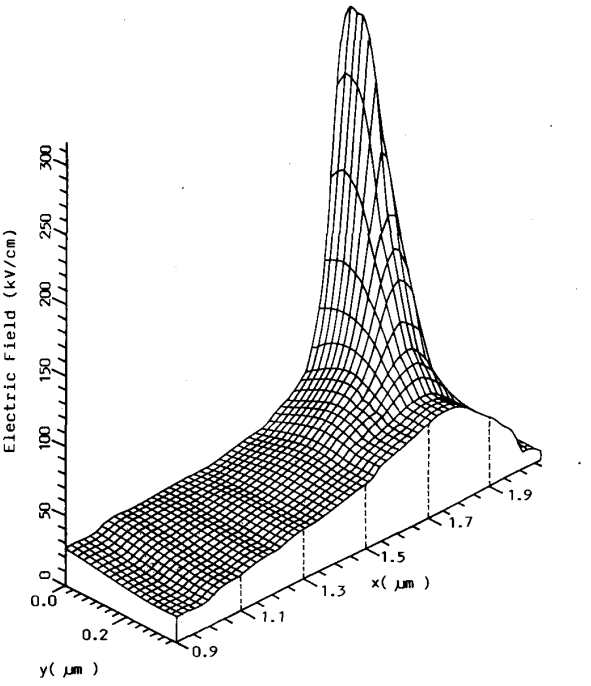

Fig. 4. The two-dimensional distribution of electric field in the channel direction in the Fig. 1 structure. $V_g = 5$ V and $V_d = 6$ V.

above the average energy. The distortion of the Maxwellian distribution in the high-field region can be realized due to the nature of nonequilibrium transport. In other words, electrons acquire a large amount of kinetic energy from a high field but cannot transform it into thermal energy through enough phonon scatterings in a short distance. Therefore, T_e' is remarkably lower than the electron temperature T_e calculated by means of $\langle E \rangle = 3/2kT_e$. In our model, T_e' is extracted in the following equation:

$$\langle E(x) \rangle' = \frac{\int_{E_1}^{\infty} E \exp(-E/kT_e') D(E)\, dE}{\int_{E_1}^{\infty} \exp(-E/kT_e') D(E)\, dE} \tag{3}$$

where $\langle E(x) \rangle'$ is computed in the EMC simulation by accumulating electrons with energy above E_1. The difference between $\langle E \rangle$ and $\langle E \rangle'$ is that $\langle E \rangle$ represents an average over the entire distribution and $\langle E \rangle'$ is the average of electrons with energy above E_1. The choice of the integration lower limit E_1 is considered in two aspects; If E_1 is chosen too large, the statistical error when computing $\langle E \rangle'$ increases due to a reduced number of sample electrons above E_1. If E_1 is chosen too small, the extracted T_e' cannot appropriately reflect the energy distribution close to the Si/SiO_2 interface barrier height. As usual, a smaller E_1 tends to overestimate T_e'. If the distribution function $f(E)$ follows strictly the Maxwellian dis-

tribution, the extracted T_e' should be exactly the same as T_e for a parabolic band structure no matter what the value of E_1 is. In the current simulation, E_1 is chosen to be 2 times the average energy. That is, $E_1(x) = c\langle E(x)\rangle$ and c is 2.

Now, the complete electron distribution can be determined by the combination of a Monte Carlo simulation and the above extrapolation technique. $f(x, E)$ in (1) is evaluated from a Monte Carlo simulation when electron energy is less than $E_1(x)$ and from the relation of

$$f(x, E) = f(x, E_1) \exp\left(-(E - E_1)/kT_e'(x)\right)$$

when E is greater than $E_1(x)$. Fig. 5 shows the EMC-calculated distribution function and our extrapolation at $x = 1.8\ \mu$m. T_e' is 1628 K, T_e is 7938 K, and E_1 is 2.04 eV. Our extrapolated distribution function (dashed line) matches the EMC result well when energy is above E_1. As a contrast, the Maxwellian distribution based on the temperature T_e (dotted line) exaggerates the distribution function significantly at high energies. It is noteworthy that the calculated value of T_e' compares favorably in orders of magnitude to the measured result (1700 K) directly from a hot-electron light emission spectrum in a 1.3-μm n-MOSFET [20]. Also shown in the inset of Fig. 5 is the corresponding energy distribution $N(E) = f(E)D(E)$.

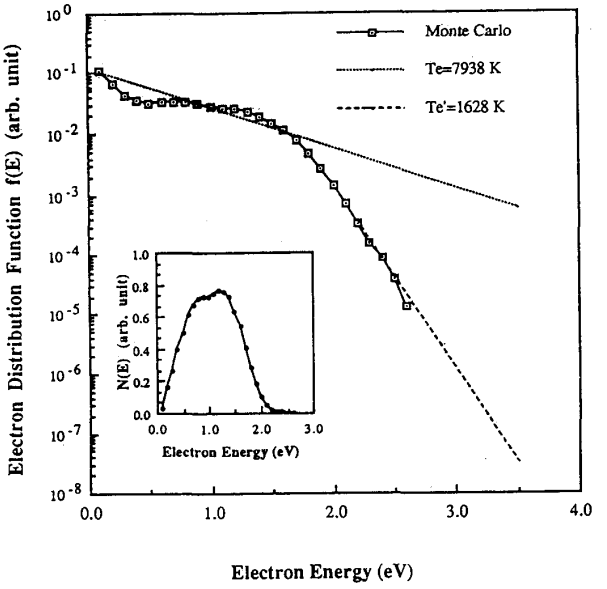

Fig. 5. Monte Carlo calculated distribution function and the extrapolated distribution at $x = 1.8\ \mu$m. The inset of the figure represents the electron energy distribution.

C. Transmission Probability in an Oxide Layer

In submicrometer MOSFET's, since the gate oxide is sufficiently thin, the lateral oxide field is much lower than the normal oxide field except for the case that the interface potential is almost equal to the gate bias. In this work, the lateral oxide field is neglected when considering the transmission probability. Two kinds of the oxide barrier geometry are plotted in Fig. 6. Fig. 6(a) represents a shape with an accelerating oxide field and Fig. 6(b) has a decelerating oxide field. Channel electrons "see" a trapezoidal barrier when their energies are lower than the barrier minimum $\phi_{\min}$ (region I in Fig. 6). The shape becomes triangular when an electron energy is higher than the barrier minimum $\phi_{\min}$ and lower than the barrier maximum $\phi_{\max}$ (region II in Fig. 6). If electrons have an energy above $\phi_{\max}$, thermionic emission is assumed (quantum reflection is ignored). The dashed lines in the figure represent the Schottky lowering effect. The electron tunneling probabilities across trapezoidal and triangular barriers using a WKB approximation are given by [21]

trapezoidal barriers:

$$T(E_y) = \exp\left\{\frac{-4\pi}{h}(2m^*)\left[\frac{2}{3q|F_y|}\right] \cdot \left[(\phi_{\max} - E_y)^{3/2} - (\phi_{\min} - E_y)^{3/2}\right]\right\}$$

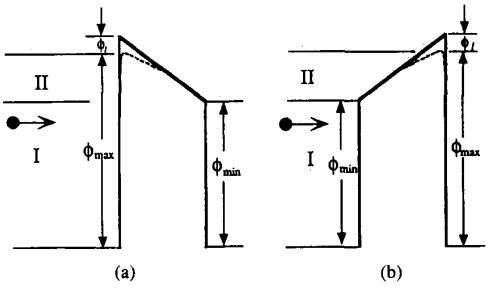

Fig. 6. Illustration of two kinds of oxide barrier geometry. Electrons are injected from the Si channel to the gate. (a) The barrier has an accelerating field. (b) The barrier has a decelerating field. ϕ_1 represents the Schottky lowering effect.

triangular barriers:

$$T(E_y) = \exp\left\{\frac{-4\pi}{h}(2m^*)\left[\frac{2}{3q|F_y|}\right](\phi_{\max} - E_y)^{3/2}\right\} \quad (4)$$

where a parabolic band structure with an effective mass $m^* = 0.5m_0$ [22] is adopted for the gate oxide layer. F_y is the normal oxide field. E_y in (4) is the energy associated with an electron whose momentum is in the y-direction. Since a parabolic band structure is used in the oxide, E_y can be written as $E\cos^2\theta$ where θ is an incident angle. Fig. 7 shows the tunneling probability across a 100-Å gate oxide as a function of electron energy at various oxide fields. The incident angle is assumed normal to the

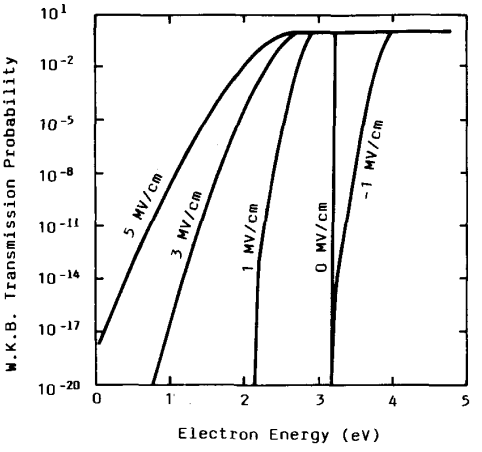

Fig. 7. The WKB tunneling probability across a 100-Å oxide versus electron energy at various oxide fields. A positive sign is defined as an accelerating field.

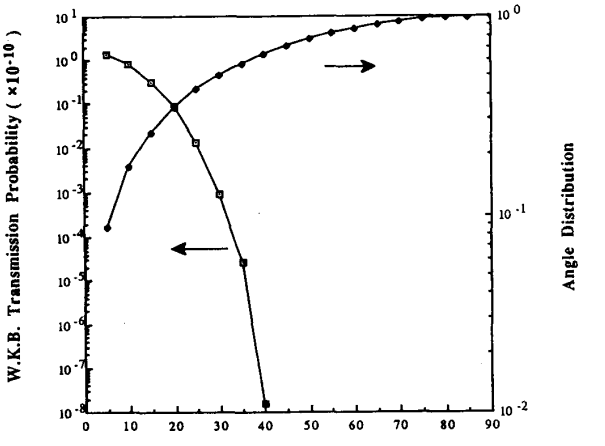

Fig. 8. The dependence of the average tunneling probability on the incident angle for a packet of Maxwellian distribution electrons. The electron temperature is 1500 K and the oxide field is 1 MV/cm.

interface. At a zero oxide field, the Si/SiO_2 interface barrier height is 3.2 eV. The tunneling probability drops immediately as the incident energy is below 3.2 eV. As the accelerating oxide field increases, the tunneling probability is enhanced due to i) the Schottky lowering and ii) the narrowing of the barrier. In order to investigate the dependence of the tunneling probability on the incident angle, the average probability $\langle T(\theta)\rangle$ is calculated in Fig. 8 for a packet of Maxwellian distributed electrons.

$$\langle T(\theta)\rangle = \int f(E)T(E\cos^2\theta)D(E)\,dE \Big/ \int f(E)D(E)\,dE. \tag{5}$$

The electron temperature is 1500 K and an oxide field of 1 MV/cm is used in Fig. 8. Since the dominant intervalley optical phonon scattering in Si has an isotropic distribution in the scattering angle, the incident angle distribution is thus proportional to $\sin\theta$. The result in Fig. 8 indicates that the tunneling probability is a sharply peaking function of the incident angle. The normal incident assumption may greatly overestimate the actual tunneling probability. Another physical process must be considered in the evaluation of the transmission probability is phonon scattering in the oxide. Following Tang's approach [7], the factor of the current loss due to scattering in the oxide is expressed as $\exp(-l/\lambda_{ox})$. $\lambda_{ox}(=32$ Å) is the electron mean free path in the oxide and l is the distance of the oxide barrier maximum from the interface. The derivation of l can be found in [7]. As a result, $P_t(x, E)$ in (1) is readily obtained as

$$P_t(x, E) = \int_0^{\pi/2} T(E\cos^2\theta)\exp(-l/\lambda_{ox})\sin\theta\,d\theta \tag{6}$$

where F_y in the expression of $T(E\cos^2\theta)$ in (4) and l are functions of x.

III. Results and Discussion

The calculated gate currents versus a gate bias V_g are compared to the measured result [23] in Fig. 9. As V_g increases toward V_d, the gate current rises due to a decrease of the decelerating oxide field (referring to Fig. 6(b)). When V_g is further increased, the gate current declines because of the reduction of a channel field heating. A bell-shaped I_g versus V_g curve results with a peak around $V_g = V_d$. In the figure, we also vary the integration lower limit $E_1 = c\langle E\rangle$ in the extrapolation. The values of c are 2.0, 2.1, and 2.2, respectively. At a lower V_g, all of the values of c converge quite well and the calculated gate currents are consistent with the measured result. A larger current fluctuation is noticed at a higher V_g for $c \doteq 2.2$. This can be understood as follows. Since the electron temperature T_e' in the high-field region is reduced at a larger V_g, it becomes more difficult to accumulate enough electrons with energy above $c\langle E\rangle$ especially when c is large. As a consequence, the statistical error and the fluctuation increase. The distribution of the CHEI current along the interface is studied in Fig. 10 at various gate biases. V_d is 6 V in the figure. The gate current has a sharp distribution in space because the electric field varies drastically along the channel. The width of the distribution increases with V_g due to the spread of the high-field region. Another point we would like to mention is that the most serious CHEI is found to be located about 200–300 Å behind the average electron energy maximum. This feature is quite different from the recent result obtained by a combined energy transport and Monte Carlo model [24]. To explain this distance, the spatial distributions of T_e and T_e' are plotted in Fig. 11. T_e' is generally lower than T_e in the high-field region as mentioned previously.

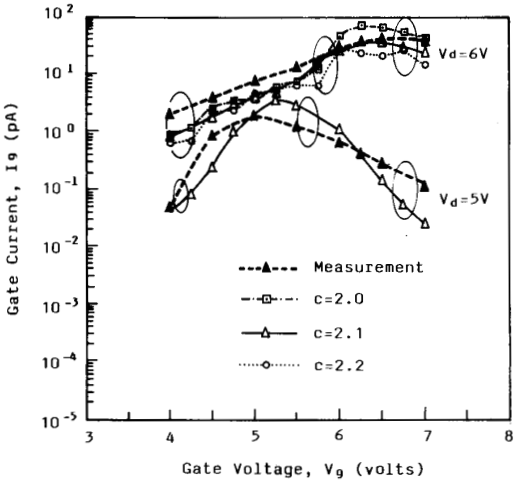

Fig. 9. Calculated and measured gate currents versus a gate bias. The measured result is from [23].

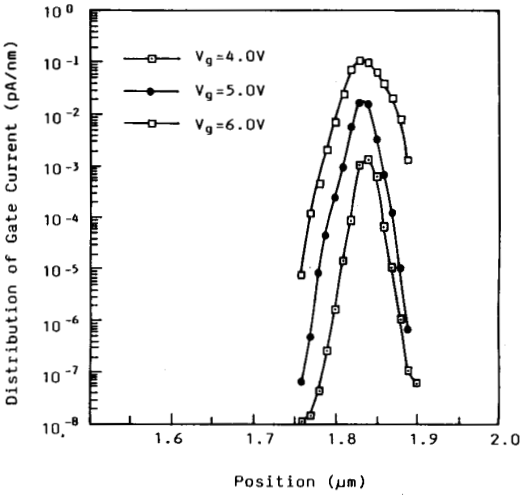

Fig. 10. The spatial distribution of the gate leakage current along the channel. V_d = 6 V.

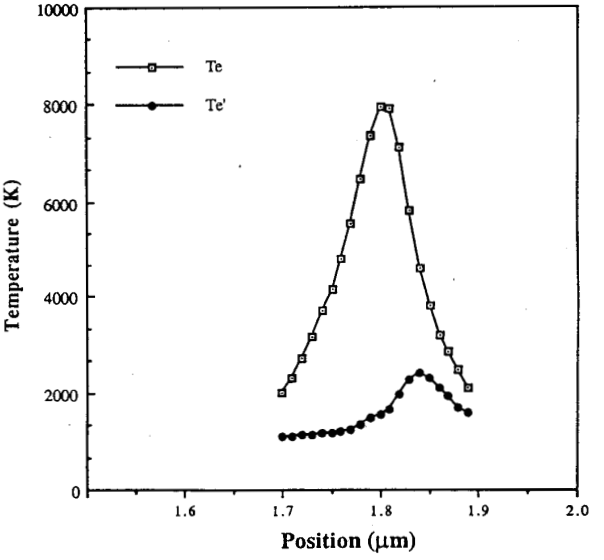

Fig. 11. The distributions of T_e and T_e' along the channel. V_d = 6 V and V_g = 5 V.

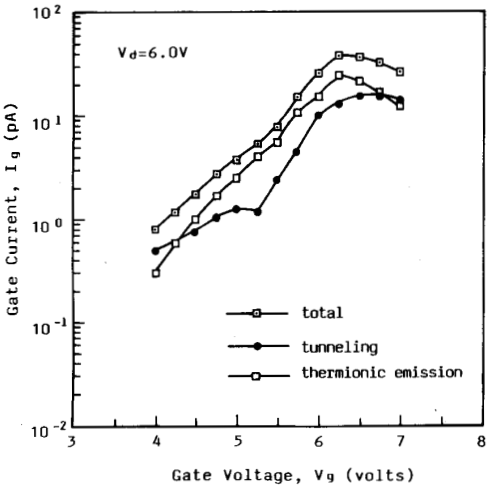

Fig. 12. Comparison of the magnitudes of thermionic emission current and quantum tunneling current as a function of a gate bias. V_d is 6 V.

At a low field, these two temperatures have a tendency to merge. However, a large discrepancy between T_e and T_e' still exists at x = 1.7 μm in the figure although the distribution function at that point is almost the Maxwellian distribution (Fig. 3). The difference arises mainly from the breakdown of the relationship $\langle E \rangle = (3/2)kT_e$ in a realistic band structure. In Fig. 11, one can notice that the maximum T_e' occurs about the above distance behind the T_e maximum. The delaying effect is believed due to a distance required to transform the acquired kinetic energy into thermal energy via phonon scatterings.

Quantum tunneling and thermionic emission in the gate current transport are compared in Fig. 12. V_d is 6 V. In the range of V_g from 4.5 to 7 V, the magnitude of the oxide field in the CHEI region, either an accelerating field or a decelerating field, is relatively small as a result of a small difference between V_g and V_d. Fig. 7 shows that the tunneling probability is minimal at a low oxide field. Therefore, the major injection process is thermionic emission in this range of V_g. Fig. 13 compares these two transport mechanisms along the channel. At V_g = 4 V, thermionic emission dominates only in the high-field region. At V_g = 6 V, the dominance of thermionic emission starts at a large heating field and extends to the overlap drain area where the potential is close to the gate bias.

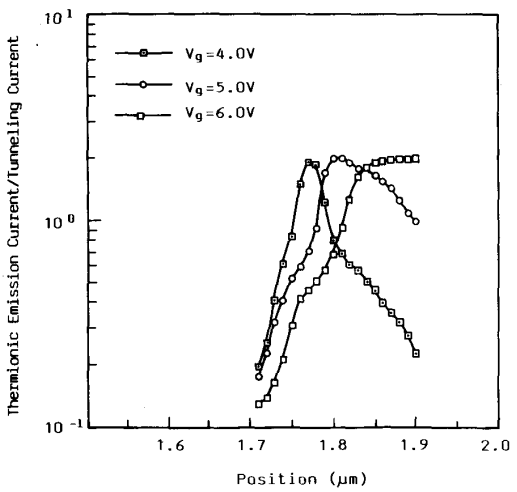

Fig. 13. The ratio of the thermionic emission current to the tunneling current along the channel at various gate biases. V_d = 6 V.

IV. Conclusions

We have developed a CHEI-caused gate leakage current model. An efficient extrapolation technique is developed to approximate the high energy tail of the distribution function. The CPU time is greatly saved by this technique. Only about 10^5 electrons are required in the EMC simulation. The model is verified by good consistency achieved between the calculated and the measured results.

References

[1] S. Tam, F-C. Hsu, C. Hu, R. S. Muller, and P. K. Ko, "Hot-electron currents in very short channel MOSFET's," *IEEE Electron Device Lett.*, vol. EDL-4, pp. 249-251, 1983.

[2] J. Hui, F-C Hsu, and J. Moll, "A new substrate and gate current phenomenon in short-channel LDD and minimum overlap devices," *IEEE Electron Device Lett.*, vol. EDL-6, pp. 135-138, 1985.

[3] A. Toriumi, M. Yoshimi, M. Iwase, and K. Taniguchi, "Experimental determination of hot-carrier energy distribution and minority carrier generation mechanism due to hot-carrier effects," in *IEDM Tech. Dig.*, 1985, pp. 56-59.

[4] T. Tsuchiya, T. Kobayashi, and S. Nakajima, "Hot-carrier-injected oxide region and hot-electron trapping as the main cause in Si n-MOSFET degradation," *IEEE Trans. Electron Devices*, vol. ED-34, pp. 386-391, 1987.

[5] P. Heremans, H. E. Maes, and N. Saks, "Evaluation of hot carrier degradation of n-channel MOSFET's with the charge pumping technique," *IEEE Electron Device Lett.*, vol. EDL-7, pp. 428-430, 1986.

[6] S. Tam, P. K. Ko, and C. Hu, "Lucky-electron model of channel hot-electron injection in MOSFET's," *IEEE Trans. Electron Devices*, vol. ED-31, pp. 1116-1126, 1984.

[7] Y. Z. Chen and T. W. Tang, "Numerical simulation of avalanche hot-carrier injection in short-channel MOSFET's," *IEEE Trans. Electron Devices*, vol. 35, pp. 2180-2188, 1988.

[8] B. Meinerzhagen, "Consistent gate and substrate current modeling based on energy transport and the lucky electron concept," in *IEDM Tech. Dig.*, 1988, pp. 504-507.

[9] D. Watanabe and S. Slamet, "Numerical simulation of hot electron phenomena," *IEEE Trans. Electron Devices*, vol. ED-30, pp. 1042-1049, 1983.

[10] R. Kuhnet, C. Werner and A. Schutz, "A novel impact ionization model for 1μm MOSFET simulation," *IEEE Trans. Electron Devices*, vol. ED-32, pp. 1057-1063, 1985.

[11] J. Frey and N. Goldsman, "Tradeoffs and electron temperature calculations in lightly doped drain structures," *IEEE Electron Device Lett.*, vol. EDL-6, pp. 28-30, 1985.

[12] K. R. Hofmann, C. Werner, W. Weber, and G. Dorda, "Hot electron and hole emission effects in short n-channel MOSFET's," *IEEE Trans. Electron Devices*, vol. ED-32, pp. 691-699, 1985.

[13] C. Fiegna, F. Venturi, M. Melanotte, E. Sangiori, and B. Riccò, "Simple and efficient modeling of EPROM writing," *IEEE Trans. Electron Devices*, vol 38, pp. 603-610, 1991.

[14] J. M. Higman, K. Hess, C. G. Hwang, and R. W. Dutton, "Coupled Monte Carlo-drift diffusion analysis of hot-electron effects in MOSFET's," *IEEE Trans. Electron Devices*, vol. 36, pp. 930-937, 1989.

[15] E. Sangiorgi, R. Pinto, F. Venturi, and W. Fichtner, "A hot-carrier analysis of submicrometer MOSFET's," *IEEE Electron Device Lett.*, vol. 9, pp. 13-15, 1988.

[16] J. Y. Tang and K. Hess, "Theory of hot electron emission from silicon into silicon dioxide," *J. Appl. Phys.*, vol. 54, pp. 5145-5151, 1983.

[17] M. Fukuma and W. Lui, "MOSFET substrate current modeling including energy transport," *IEEE Electron Device Lett.*, vol. EDL-8, pp. 214-216, 1987.

[18] M. R. Pinto, C. S. Rafferty, H. R. Yeager, and R. W. Duntton, "PISCES-IIB Poisson and Continuity Equation Solver," Stanford Electrons Lab., Stanford Univ., Palo Alto, CA, Feb. 1986.

[19] L. V. Keldysh, "Concerning the theory of impact ionization in semiconductors," *Sov. Phys.—JETP*, vol. 21, pp. 1135-1144, 1965.

[20] M. Lanzoni, E. Sangiorgi, C. Fiegna, M. Manfredi, and B. Riccò, "Extended (1.1-2.9 eV) hot-carrier induced photon emission in n-channel MOSFET's," in *IEDM Tech. Dig.*, 1990, pp. 69-72.

[21] K. M. Chu and D. L. Pulfrey, "An improved model for metal-insulator-semiconductor tunnel junction," *IEEE Trans. Electron Devices*, vol. 35, pp. 1656-1663, 1988.

[22] D. R. Young, "Electron current injected into SiO_2 from p-type Si depletion regions," *J. Appl. Phys.*, vol. 47, pp. 2098-2102, 1976.

[23] E. Takeda, Y. Nakagome, H. Kume, and S. Asai, "New hot-carrier injection and device degradation in submicron MOSFET's," *Proc. Inst. Elec. Eng*, pt. I, vol. 130, pp. 144-150, 1983.

[24] S. L. Wang, N. Goldsman, L. Henrickson, and J. Frey, "MOSFET hot-electron gate current calculation by combining energy transport method with Monte Carlo simulation," in *IEDM Tech. Dig.*, 1990, pp. 447-450.

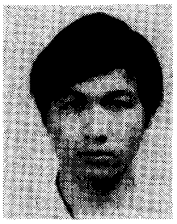

Chimoon Huang was born in Chang-Hua, Taiwan, on October 15, 1964. He received the B.S. degree in electrical engineering from National Taiwan Ocean University in 1986. Currently, he is working towards the Ph.D. degree in electrical engineering at National Chiao-Tung University.

His current research interest is in the modeling and simulation of hot-carrier effects in submicrometer semiconductor devices.

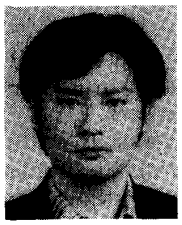

Tahui Wang was born in Taoyuan, Taiwan, on May 3, 1958. He received the B.S. and Ph.D. degrees in electrical engineering from National Taiwan University and the University of Illinois in 1980 and 1985, respectively.

From 1985 to 1987, he was with the High-Speed Devices Laboratory of Hewlett-Packard Labs, where he was engaged in the research and development of compound semiconductor devices and circuits. Currently, he is a Full Professor at the Institute of Electronics, National Chiao-Tung University. His current research interest is in the modeling and simulation of semiconductor devices and circuits.

C. N. Chen, photograph and biography not available at the time of publication.

M. C. Chang, photograph and biography not available at the time of publication.

J. Fu, photograph and biography not available at the time of publication.